Wrinkling of monolayer graphene: A study by molecular dynamics and continuum plate theory

C. Y. Wang,[1] K. Mylvaganam,[2] and L. C. Zhang[2,*]
[1]*School of Engineering, Swansea University, Singleton Park, Swansea, SA2 8PP Wales, United Kingdom*
[2]*School of Mechanical and Manufacturing Engineering, The University of New South Wales, New South Wales 2052, Australia*
(Received 3 June 2009; published 23 October 2009)

Wrinkling was observed for a circular monolayer graphene sheet in nanoindentation based on molecular-dynamics simulations. The mechanics fundamentals of this phenomenon were then explored using a two-dimensional plate model. It was found that the graphene wrinkles when the indentation depth reaches a critical value, the wrinkling is induced by the circumferential compression in the graphene, and the bending stiffness of the graphene sheet plays an essential role in stabilizing its one-atom layer nanostructures. It was shown that bending stiffness and in-plane stiffness are key indicators that signify the intrinsic mechanical properties of a graphene.

DOI: 10.1103/PhysRevB.80.155445 PACS number(s): 61.46.−w, 31.15.xv, 62.25.−g

I. INTRODUCTION

Since the late 1980s, nanoscale carbon materials, such as bucky balls[1] and carbon nanotubes (CNTs),[2,3] have been found to have superior mechanical, electrical, and thermal properties to many classical materials. This has led to extensive discussions about the potential applications of these carbon materials[1,4,5] and has brought about a significant wave of investigations for a precise characterization of their properties.[6–11] Recently, a new member of carbon family, monolayer graphene flakes, has been synthesized[12] and their mechanical properties have attracted considerable attention.[13–22] It was reported[15] that the graphene flakes could be the strongest material ever obtained in terms of their elastic stiffness and fracture strength. They can also be used as nanoresonators with the vibration frequency up to terahertz.[17,19,21] On the other hand, Meyer *et al.*[23] in their TEM study reported the rippled surface, caused by the structural instability, of a suspended graphene, which can significantly degrade the Dirac spectrum and electronic properties of the graphene. Hence, understanding the mechanics of the structural instability of a graphene is of primary importance.[23–26] This, however, requires that a suitable mechanics analysis be carried out to reveal the deformation mechanisms and capture the key factors that are responsible for the structural instability of a graphene.

There are some critical fundamental issues with respect to the validity of the characterization methods used that could have incorrectly estimated the mechanical properties of a monolayer graphene. For example, in their nanoindentation studies, Lee, *et al.*[14] treated a suspended graphene sheet as a membrane of a fictitious thickness without any bending resistance, but Hemmasizadeh[15] and Dun and Wang[22] considered the sheet as a thin plate with a nonzero bending stiffness, leading to different mechanics interpretations. Lee *et al.*[14] explained that the linear term in equation $p=\lambda(w_0)+\kappa(w_0)^3$ (p is the transverse load, w_0 is indentation depth defined as the transverse displacement at the center of the graphene tested, and λ and κ are real coefficients) was a result of the high residual stress in the graphene. However, Hemmasizadeh[14] concluded that it was due to the contribution of the graphene's bending stiffness. In addition, when using a continuum mechanics theory to analyze a monolayer graphene, e.g., an elastic membrane or an elastic thin plate theory, there are conceptual problems such as the "effective thickness" and "effective Young's modulus" as have been extensively addressed in the mechanical characterization of single-walled carbon nanotubes.[6,10,11,27] These "effective quantities" in continuum mechanics may not exist at the nanoscopic scale for describing the properties of a carbon nanomaterial because the conventional continuum mechanics does not involve the atomic structure of a material, and, in principle, is not applicable to a nanoscale structure since the fundamental assumptions on which the continuum mechanics theory is based (e.g., the continuity of a material) is no longer valid at the nanoscopic scale. Thus to correctly interpret the experimental observations,[15,23,24] it is essential to find out proper indicators that can reflect correctly the intrinsic properties of a graphene.

II. MOLECULAR-DYNAMICS SIMULATION

Motivated by the aforementioned earlier studies we have performed a nanoindentation on a circular graphene sheet based on molecular-dynamics (MD) simulation, an essential theoretical tool for property characterization of nanomaterials.[28–33] It has been shown that MD can provide an accurate description to the buckling[29,34] and vibration properties[35,36] of CNTs, and the phase transformation behavior of silicon.[37] As a result, it has often been utilized as a reference to validate the equivalent continuum mechanics models for nanomaterials, where the atomic structures of the materials are ignored.[28,38,39] In our MD analysis, the interactions between the graphene carbon atoms were modeled by the Tersoff-Brenner potential[40,41] and the interactions between the diamond indenter tip and the graphene were modeled by the Lennard-Jones potential.[42] As pointed out in our previous study[43] on CNTs, a proper use of a thermostat scheme in an MD simulation is critical to producing meaningful results. Therefore in this work, we applied Berendsen thermostat on all the atoms and kept the simulation at the temperature of 300 K.

In the nanoindentation (Fig. 1), a load is applied by an indenter tip of diameter 0.535 nm at the center of a circular

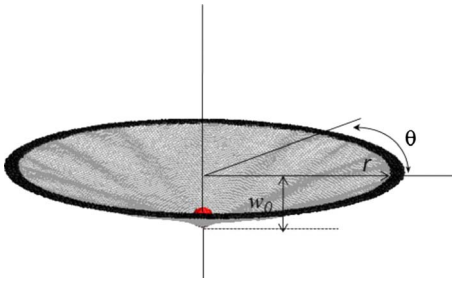

FIG. 1. (Color online) Side view of a circular graphene at an indentation depth of w_0=4.5 nm; simply supported boundary atoms are shown in black.

graphene of radius 16 nm. This load can be reasonably considered as a point load because the indenter diameter is much smaller than that of the graphene sheet. The boundary of the graphene is simply supported, i.e., the boundary atoms cannot move in the direction normal to the r-θ plane (Fig. 1), but can move freely within the plane, where r is the radial coordinate and θ is the circumferential angular coordinate. The simulation showed that the indentation depth (w_0) increases with the rising indentation force (p). When w_0 reaches a critical value of around 0.7 nm, wrinkling, i.e., the ripplelike transverse deflection, suddenly emerges. The wrinkling displacement at w_0=1.1 nm is shown in Fig. 2(a) as a function of r and θ, which demonstrates that the ripplelike deflection is (almost) zero in the vicinity of the graphene center (r=0), increases with the increment of r, and reaches its maximum in the interval of r=9–11 nm. The wrinkling displacement then decreases monotonically to zero at the simply supported boundary of the graphene (r=16 nm). A further increment of w_0 after the initial wrinkling leads to greater ripplelike displacements and a larger number of waves (ripples) in the circumferential direction [Fig. 2(b)]. The postwrinkling mode (at w_0=8.2 nm) predicted by the MD simulation is shown in Fig. 3. Here the MD simulation indicates that the graphene behaves fundamentally differently from a membrane without a bending stiffness, because a membrane would wrinkle whenever a compressive stress is generated and does not have a critical wrinkling load.[44] Such an initial wrinkling behavior predicted based on MD simulation is in agreement with the recent experiment observation that there exists a critical wrinkling load for graphene.[45] It is thus concluded that a thin elastic plate theory with a nonzero bending stiffness is more appropriate than a membrane. This implication is consistent with the analyses of CNTs,[11,46] where single-walled CNTs as curved graphene sheets are found to be approximately equivalent to elastic thin shells. These unique features necessitate an investigation into the mechanics of the graphene wrinkling detailed below, which will develop a suitable mechanics model for graphene sheet and provide essential information for clarifying the fundamental issues in characterizing monolayer carbon nanomaterials under the umbrella of continuum mechanics.

III. CONTINUUM MECHANICS ANALYSIS

It has been shown that the deformation of a graphene sheet is controlled by four stiffnesses via a set of two-

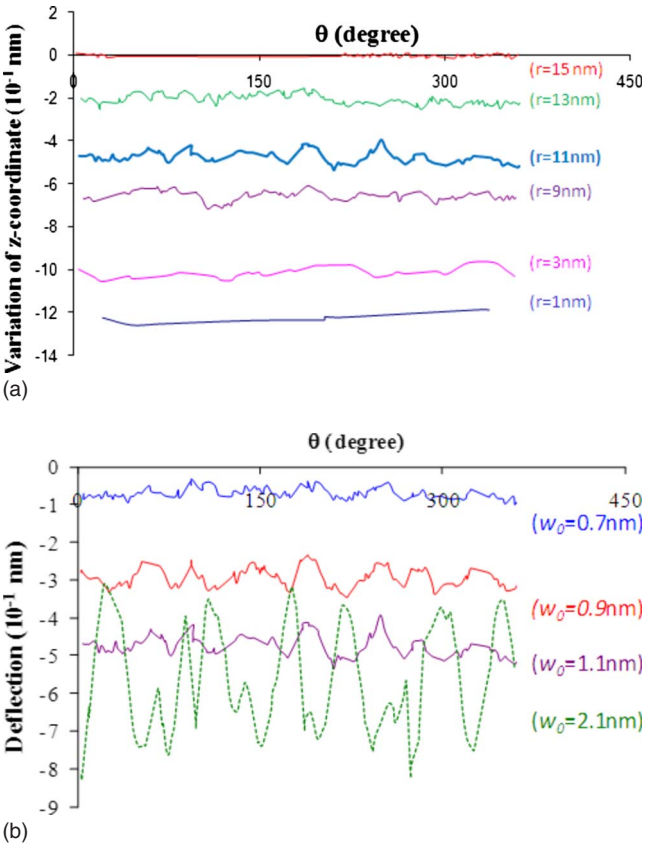

FIG. 2. (Color online) Wrinkling displacement observed in MD simulation. (a) The distribution of wrinkling displacement when r increases from 1 to 15 nm, which is recorded when w_0=1.1 nm. (b) The wrinkling displacement at r=11 nm and θ=0°–360°, which increases when indentation depth w_0 rises from 0.7 to 2.1 nm.

dimensional (2D) constitutive relations:[11,27,46] in-plane extension stiffness $K_{\text{extension}}$, in-plane torsion stiffness K_{torsion}, bending stiffness D_{bending}, and off-plane torsion stiffness D_{torsion}, which can be measured directly in atomistic simulations without defining the effective thickness of the graphene. D_{bending} and D_{torsion} quantify the resistance of a graphene to the changes of the off-plane π bonds due to off-plane deformation (e.g., bending), while $K_{\text{extension}}$ and

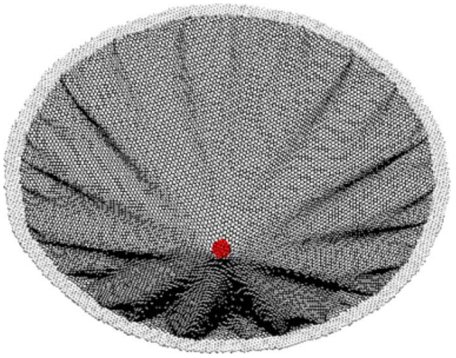

FIG. 3. (Color online) The wrinkling mode of a simply supported monolayer graphene under a central indentation predicted by MD simulation. Note the deflection is enlarged for illustration purpose.

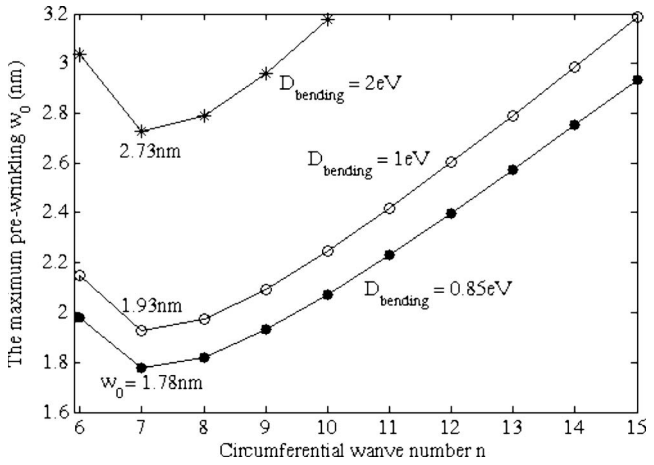

FIG. 4. The value of prewrinkling indentation depth w_0 against the corresponding circumferential wave number n of wrinkling. For bending stiffness D_{bending}=0.85 eV, 1 eV and 2 eV (Ref. 10) the critical wrinkling value of w_0 increases from 1.78 nm, to 1.93 nm, and to 2.73 nm.

K_{torsion} reflect its resistance to the variation in the in-plane σ bonds induced by in-plane deformation (e.g., in-plane stretching).[11,46,47] These deformation mechanisms are substantially different from those of a three-dimensional (3D) thin plates/shell where the in-plane stretching is uniformly distributed across plate/shell thickness and the bending is caused by the linearly distributed stresses across the thickness. Consequently, the four elastic stiffnesses of graphene sheets do not necessarily satisfy the compatibility condition of a 3D continuum plate/shell structure, $K_{\text{extension}}/D_{\text{bending}} = K_{\text{torsion}}/D_{\text{torsion}}$, which is the existence condition of well-defined effective thickness and equivalent Young's modulus of one-atom layer nanostructures.[11] In other words, a monolayer graphene may not have an effective thickness or an effective Young's modulus.[10,11] This also means that it is the unique deformation mechanisms of a discrete material, rather than its material discontinuity, that limit the applicability of a 3D continuum mechanics theory in nanomechanics. Therefore, in this paper a monolayer graphene will be treated as a 2D material whose intrinsic mechanical properties are characterized by the above four independent material constants. In what follows, this 2D plate model will be employed for the wrinkling analysis of the graphene studied by the MD simulation introduced above, where the deformation is primarily determined by the material constants D_{bending} and $K_{\text{extension}}$.

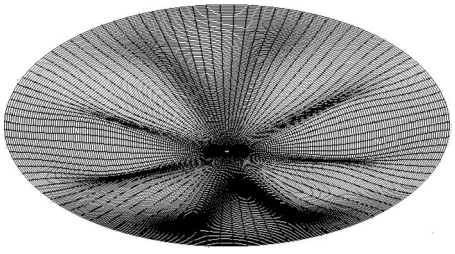

FIG. 5. The wrinkling mode predicted by the 2D plate model.

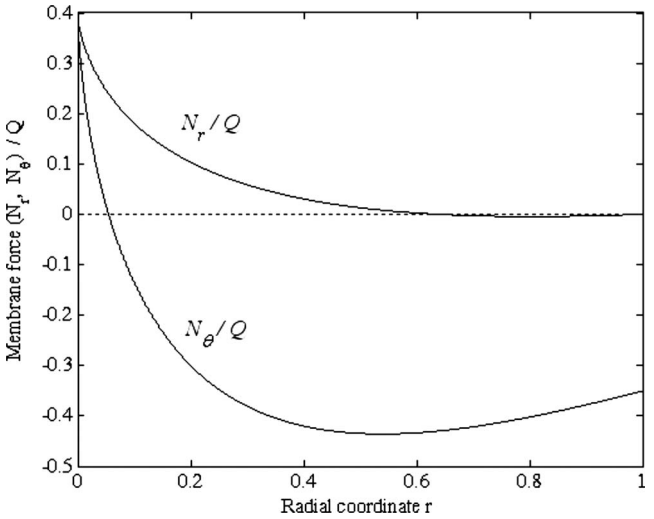

FIG. 6. The distribution of prewrinkling axis-symmetric membrane forces N_r and N_θ of a simply supported circular graphene sheet whose boundary is free to move in r-θ plane. Here $Q = (K_{\text{extension}} \cdot w_0^2)/R^2$.

When using the energy method considering both stretching and bending of the graphene, the condition for the onset of wrinkling is[48]

$$\Delta W = \Delta U, \tag{1}$$

where $\Delta W = \Delta W_1 + \Delta W_2$ in which ΔW_1 is the work done by the in-plane forces at the graphene boundary and ΔW_2 is the work done by the transverse forces and bending moments. In Eq. (1), $\Delta U = \Delta U_1 + \Delta U_2 + \Delta U_3$, where ΔU_1 and ΔU_2 are the stretching energy due to the in-plane and off-plane displacements, respectively, and ΔU_3 is the energy due to bending. Under the present loading and boundary conditions, $\Delta W_1 = \Delta U_1$ (Ref. 48) and $\Delta W_2 = 0$. The latter is true because no bending moment is applied and the transverse displacement due to *initial* wrinkling is zero at the center[49] [also see in Fig. 2(a)] and at the graphene boundary. Equation (1) then reduces to

$$\Delta U_2 + \Delta U_3 = 0, \tag{2}$$

where

$$\Delta U_2 = \frac{1}{2}\int\int \left\{ N_r \left(\frac{\partial w}{\partial r}\right)^2 + N_\theta \left(\frac{1}{r}\frac{\partial w}{\partial \theta}\right)^2 \right\},$$

$$\Delta U_3 = \int\int \left[\frac{D}{2}\left(\frac{\partial^2 w}{\partial r^2} + \frac{1}{r}\frac{\partial w}{\partial r} + \frac{1}{r^2}\frac{\partial^2 w}{\partial \theta^2}\right)^2 - D(1-\nu)\frac{\partial^2 w}{\partial r^2}\left(\frac{1}{r}\frac{\partial w}{\partial r} + \frac{1}{r^2}\frac{\partial^2 w}{\partial \theta^2}\right) + D(1-\nu)\left(\frac{1}{r}\frac{\partial^2 w}{\partial r\,\partial\theta} - \frac{1}{r^2}\frac{\partial w}{\partial \theta}\right)^2 \right] r dr d\theta,$$

and $N_r(\alpha, w_o)$ and $N_\theta(\alpha, w_o)$ (where $\alpha = r/R$) (Appendix A of Ref. 50) are the radial and circumferential membrane forces at the onset of wrinkling.[48,51] Based on the wrinkling mode predicted by the MD simulation described above, it is rea-

sonable to assume that the wrinkling displacement for the energy calculation in Eq. (2) is $w=Af(\alpha,\theta)$, where A is a displacement amplitude. This wrinkling displacement distribution satisfies the simply supported boundary conditions enforced on the graphene. Substituting $N_x(\alpha,w_0)$, $N_\theta(\alpha,w_0)$, and $w(\alpha,\theta)$ into Eq. (2) yields (Appendix B of Ref. 50)

$$(w_0)_{cr} = B\sqrt{\frac{D_{\text{bending}}}{K_{\text{extension}}}}, \tag{3}$$

where $(w_o)_{cr}$ represents the critical value of w_o at the onset of wrinkling; B is a coefficient varying with the imposed boundary condition. Equation (3) shows that $(w_o)_{cr}$ is determined by $D_{\text{bending}}/K_{\text{extension}}$ but independent of the graphene radius R. This is in accordance with the numerical results[49] based on the von Karman plate theory[22] for circular plates. It then follows that the small but nonzero bending stiffness plays a vital role in maintaining the structural stability of a graphene. Note that the von Karman plate theory[22,49] could be more accurate for analyzing a graphene,[22] but this theory will lead to nonlinear differential equations that can only be solved numerically[49] and cannot bring about an explicit formula like Eq. (3).

Now let us choose a specific approximate wrinkling displacement, $w=Af(\alpha,\theta)$, to predict the critical value $(w_o)_{cr}$ and the associated initial wrinkling mode of the graphene. Let

$$w = A\left(\frac{r}{R}\right)^4\left[\left(\frac{r}{R}\right)-1\right]^3\cos n\theta. \tag{4}$$

Note that w is perpendicular to the r-θ plane and does not include the prewrinkling deflection of the graphene. In Eq. (4), n is the circumferential wave number of the wrinkling mode. Equation (4) satisfies the simply supported boundary condition $[w|_{r=R}=0$ and $[(\nu dw/rdr)+(d^2w/dr^2)]|_{r=R}=0$ (Refs. 48, 49, and 51)] and the condition $w|_{r=0}=0$,[49] but does not directly define a freely movable boundary in the r-θ plane. Clearly, Eq. (4) gives the trend of $w(r)$ similar to the prediction of MD for initial and postwrinkling of the graphene [Fig. 2(a)]. The maximum w according to Eq. (4) is at $r\approx 9$ nm for a circular graphene of $R=16$ nm, which is close to 9 to 11 nm given by the MD simulation. Equation (4) thus forms a reasonable approximation for the initial wrinkling modes of the graphene. Substituting Eq. (4) into Eq. (2) gives the minimum value $(w_0)_{cr}=1.78-2.73$ nm with $n=7$ as shown in Fig. 4. In the calculation $D_{\text{bending}}=0.85$, 1, and 2 eV and $K_{\text{extension}}=340$ GPa/nm according to Refs. 10 and 15. The corresponding wrinkling mode predicted by this 2D plate model is shown in Fig. 5, which is consistent with the MD prediction of seven to eight waves at the emergence of wrinkling (Fig. 2(b) and 3). This shows the validity of the present 2D plate model for the wrinkling analysis of the monolayer graphene.

To further identify the origin of the wrinkling we have plotted in Fig. 6 the prewrinkling forces N_r and N_θ (Appendix A of Ref. 50). We can see that N_r is positive in the range of $r<0.6R$ and close to zero when $0.6R\le r\le R$. Positive N_θ is also found at $r<0.06R$. However, at $0.06R\le r\le R$ N_θ is negative. These indicate that prior to wrinkling the graphene is primarily stretched out in the radial direction but mainly compressed in the circumferential direction due to its perimeter reduction when the material is pulled to the its center by the nanoindentation. The compression increases linearly with w_0^2 (Appendix A of Ref. 50). Specifically, the monolayer graphene during postwrinkling deformation can withstand a great deal of compressive stress due to its bending stiffness.

IV. CONCLUSIONS

This study concludes that wrinkling occurs in a simply supported circular graphene under a central point load when the indentation depth w_0 reaches a critical value. Increasing the indentation depth will further develop the wrinkling with growing displacement and number of circumferential waves. The 2D plate model demonstrates that such wrinkling is initiated by the circumferential compressive force with the critical value of w_0 solely determined by the bending stiffness-to-extension stiffness ratio $D_{\text{bending}}/K_{\text{extension}}$. From these results it follows that bending stiffness D_{bending} and in-plane stiffness $K_{\text{extension}}$ of graphene are two key material properties that largely determines the resistance of graphene to the structural instability.

*Corresponding author; liangchi.zhang@unsw.edu.au

[1] H. W. Kroto, J. R. Heath, S. C. O'Brien, R. F. Curl, and R. E. Smalley, Nature (London) **318**, 162 (1985).
[2] S. Iijima, Nature (London) **354**, 56 (1991).
[3] T. W. Ebbesen and P. M. Ajayan, Nature (London) **358**, 220 (1992).
[4] P. Ball, Nature (London) **414**, 142 (2001).
[5] R. H. Baughman, A. A. Zakhidov, and W. A. de Heer, Science **297**, 787 (2002).
[6] T. Vodenitcharova and L. C. Zhang, Phys. Rev. B **68**, 165401 (2003).
[7] T. Vodenitcharova and L. C. Zhang, Phys. Rev. B **69**, 115410 (2004).
[8] R. F. Gibson, E. O. Avorinde, and Y. F. Wen, Compos. Sci. Technol. **67**, 1 (2007).
[9] C. Y. Wang, Y. Y. Zhang, C. M. Wang, and V. B. C. Tan, J. Nanosci. Nanotechnol. **7**, 4221 (2007).
[10] C. Y. Wang and L. C. Zhang, Nanotechnology **19**, 075705 (2008).
[11] C. Y. Wang and L. C. Zhang, Nanotechnology **19**, 195704 (2008).
[12] K. S. Novoselov, A. K. Geim, S. V. Morozov, D. Jiang, Y. Zhang, S. V. Dubonos, I. V. Grigorieva, and A. A. Firsov, Science **306**, 666 (2004).
[13] S. N. Medyanik, E. G. Karpov, and W. K. Liu, J. Comput. Phys. **218**, 836 (2006).
[14] C. G. Lee, X. D. Wei, J. W. Kysar, and J. Hone, Science **321**, 385 (2008).

[15] A. Hemmasizadeh, M. Mahzoon, E. Hadi, and R. Khandan, Thin Solid Films **516**, 7636 (2008).
[16] C. Gomez-Navarro, M. Burghard, and K. Kern, Nano Lett. **8**, 2045 (2008).
[17] D. Garcia-Sanchez, A. M. Van der Zande, A. San Paulo, B. Lassagne, P. L. McEuen, and A. Bachtold, Nano Lett. **8**, 1399 (2008).
[18] H. C. Schniepp, K. N. Kudin, J. L. Li, R. K. Prudhomme, R. Car, D. A. Saville, and I. A. Aksay, ACS Nano **2**, 2577 (2008).
[19] N. L. Rangel and J. M. Seminario, J. Phys. Chem. A **112**, 13699 (2008).
[20] C. D. Reddy, A. Ramasubramaniam, V. B. Shenoy, and Y. Y. Zhang, Appl. Phys. Lett. **94**, 101904 (2009).
[21] T. Murmu and S. C. Pradhan, J. Appl. Phys. **105**, 064319 (2009).
[22] W. H. Duan and C. M. Wang, Nanotechnology **20**, 075702 (2009).
[23] J. C. Meyer, A. K. Geim, M. I. Katsnelson, K. S. Novoselov, T. J. Booth, and S. Roth, Nature (London) **446**, 60 (2007).
[24] A. Fasolino, J. H. Los, and M. I. Katsnelson, Nat. Mater. **6**, 858 (2007).
[25] N. Abedpour, M. Neek-Amal, R. Asgari, F. Shahbazi, N. Nafari, and M. Reza Rahimi Tabar, Phys. Rev. B **76**, 195407 (2007).
[26] E. A. Kim and A. H. C. Neto, EPL **84**, 57007 (2008).
[27] Y. Huang, J. Wu, and K. C. Hwang, Phys. Rev. B **74**, 245413 (2006).
[28] B. I. Yakobson, C. J. Brabec, and J. Bernholc, Phys. Rev. Lett. **76**, 2511 (1996).
[29] S. Iijima, C. Brabec, A. Maiti, and J. Bernholc, J. Chem. Phys. **104**, 2089 (1996).
[30] V. N. Popov and L. Henrard, Phys. Rev. B **65**, 235415 (2002).
[31] K. M. Liew, C. H. Wong, X. Q. He, M. J. Tan, and S. A. Meguid, Phys. Rev. B **69**, 115429 (2004).
[32] C. P. Herrero and R. Ramirez, Phys. Rev. B **79**, 115429 (2009).
[33] P. Liu and Y. W. Zhang, Appl. Phys. Lett. **94**, 231912 (2009).
[34] Y. R. Jeng, P. C. Tsai, and T. H. Fang, Appl. Phys. Lett. **90**, 161913 (2007).
[35] A. M. Rao, E. Richter, S. Bandow, B. Chase, P. C. Eklund, K. A. Williams, S. Fang, K. R. Subbaswamy, M. Menon, A. Thess, R. E. Smalley, G. Dresselhaus, and M. S. Dresselhaus, Science **275**, 187 (1997).
[36] U. D. Venkateswaran, A. M. Rao, E. Richter, M. Menon, A. Rinzler, R. E. Smalley, and P. C. Eklund, Phys. Rev. B **59**, 10928 (1999).
[37] K. Mylvaganam, L. C. Zhang, P. Eyben, J. Mody, and W. Vandervorst, Nanotechnology **20**, 305705 (2009).
[38] C. Y. Wang, C. Q. Ru, and A. Mioduchowski, J. Appl. Phys. **97**, 024310 (2005).
[39] A. Sears and R. C. Batra, Phys. Rev. B **73**, 085410 (2006).
[40] D. W. Brenner, Phys. Rev. B **42**, 9458 (1990).
[41] D. W. Brenner, O. A. Shenderova, J. Harrison, S. J. Stuart, B. Ni, and S. B. Sinnott, J. Phys.: Condens. Matter **14**, 783 (2002).
[42] M. P. Allen and D. J. Tildesley, *Computer Simulation of Liquids* (Clarendon Press, Oxford, 1987), p. 21.
[43] K. Mylvaganam and L. C. Zhang, Carbon **42**, 2025 (2004).
[44] C. Jin and X. D. Wang, J. Mech. Phys. Solids **56**, 2815 (2008).
[45] C. G. Lee, X. D. Wei, J. W. Kysar, and J. Hone (unpublished).
[46] Z. C. Tu and Z. C. Ou-Yang, Phys. Rev. B **65**, 233407 (2002).
[47] G. M. Odegard, T. S. Gates, L. M. Nicholson, and K. E. Wise, Compos. Sci. Technol. **62**, 1869 (2002).
[48] S. P. Timoshenko and J. M. Gere, *Theory of Elastic Stability* (McGraw-Hill, New York, 1961).
[49] G. G. Adams, J. Appl. Mech. **60**, 520 (1993).
[50] See EPAPS Document No. E-PRBMDO-80-048939 for the derivation of the formulas shown in Sec. III (continuum mechanics analysis). For more information on EPAPS, see http://www.aip.org/pubservs/epaps.html.
[51] S. P. Timoshenko, *Theory of Plates and Shells* (McGraw-Hill, New York, 1940).